J|A|C|S ARTICLES

Published on Web 03/12/2009

Phase Transformation of Biphasic $Cu_2S-CuInS_2$ to Monophasic $CuInS_2$ Nanorods

Stephen T. Connor,[†] Ching-Mei Hsu,[‡] Benjamin D. Weil,[‡] Shaul Aloni,[§] and Yi Cui*[,‡]

Departments of Chemistry and of Materials Science and Engineering, Stanford University, Stanford, California 94305, and Molecular Foundry, Materials Science Division, Lawrence Berkeley National Laboratory, Berkeley, California 94720

Received December 25, 2008; E-mail: yicui@stanford.edu

Abstract: We synthesized wurtzite $CuInS_2$ nanorods (NRs) by colloidal solution-phase growth. We discovered that the growth process starts with nucleation of Cu_2S nanodisks, followed by epitaxial overgrowth of $CuInS_2$ NRs onto only one face of Cu_2S nanodisks, resulting in biphasic $Cu_2S-CISu$ heterostructured NRs. The phase transformation of biphasic $Cu_2S-CuInS_2$ into monophasic $CuInS_2$ NRs occurred with growth progression. The observed epitaxial overgrowth and phase transformation is facile for three reasons. First, the sharing of the sulfur sublattice by the hexagonal chalcocite Cu_2S and wurtzite $CuInS_2$ minimizes the lattice distortion. Second, Cu_2S is in a superionic conducting state at the growth temperature of 250 °C wherein the copper ions move fluidly. Third, the size of the Cu_2S nanodisks is small, resulting in fast phase transformation. Our results provide valuable insight into the controlled solution growth of ternary chalcogenide nanoparticles and will aid in the development of solar cells using ternary $I-III-VI_2$ semiconductors.

Introduction

Ternary $I-III-VI_2$ semiconductors have garnered great interest due to their promise for photovoltaic applications. The $I-III-VI_2$ class of materials has myriad benefits, including large absorption coefficients and good stability under solar radiation.[1] Thin films of $CuIn_xGa_{1-x}Se_2$ (CIGS) with a band gap of 1.3 eV have been demonstrated to have a high power efficiency of ~20%, which is the highest among thin-film solar cell technologies. An analogous system, $CuInS_2$ (CISu), has a desirable direct band gap of 1.5 eV, which is also well matched with the solar spectrum and is more environmentally friendly without Se.[2] Theoretical solar conversion efficiencies of 27−32% have been calculated with CISu as an absorber,[3,4] and CISu thin film solar cells of 12% efficiency have been successfully made.[4] However, these CIGS and CISu solar cells are typically fabricated via a high-cost vacuum coevaporation process,[5] but a low-cost process is desired.

Recently, colloidal nanocrystals of solar absorber materials have attracted much attention.[6−11] Nanocrystal syntheses can utilize lower processing temperatures than bulk synthesis methods, and device fabrication with nanocrystals can benefit from roll to roll processing and solution-phase processing such as printing.[12] In addition, we have recently shown that chemically synthesized nanostructures can generally provide well-defined domains for understanding complex phase behaviors such as vacancy ordering and Cu(I) ion diffusion,[13,14] which are particularly important in $I-III-VI_2$ semiconductors.

CISu nanocrystals have previously been made by standard synthetic methods such as solvothermal techniques,[15,16] hydrothermal techniques,[17] and single-source decomposition.[18,19] Nanocrystals have been most commonly synthesized as the

[†] Department of Chemistry, Stanford University.
[‡] Department of Materials Science and Engineering, Stanford University.
[§] Lawrence Berkeley National Laboratory.

(1) Lewerenz, H. J. *Sol. Energy Mater. Sol. Cells* **2004**, *83*, 395–407.
(2) Yoshino, K.; Ikari, T.; Shirakata, S.; Miyake, H.; Hiramatsu, K. *Appl. Phys. Lett.* **2001**, *78*, 742–744.
(3) Meese, J. M.; Manthuruthil, J. C.; Locker, D. R. *Bull. Am. Phys. Soc.* **1975**, *20*, 696–697.
(4) Braunger, D.; Hariskos, D.; Walter, T.; Schock, H. W. *Sol. Energy Mater. Sol. Cells* **1996**, *40*, 97–102.
(5) Wu, Y. L.; Lin, H. Y.; Sun, C. Y.; Yang, M. H.; Hwang, H. L. *Thin Solid Films* **1989**, *168*, 113–122.
(6) Kim, S.; Fisher, B.; Eisler, H. J.; Bawendi, M. *J. Am. Chem. Soc.* **2003**, *125*, 11466–11467.
(7) Robel, I.; Subramanian, V.; Kuno, M.; Kamat, P. V. *J. Am. Chem. Soc.* **2006**, *128*, 2385–2393.
(8) Wang, P.; Abrusci, A.; Wong, H. M. P.; Svensson, M.; Andersson, M. R.; Greenham, N. C. *Nano Lett.* **2006**, *6*, 1789–1793.
(9) Wu, Y.; Wadia, C.; Ma, W. L.; Sadtler, B.; Alivisatos, A. P. *Nano Lett.* **2008**, *8*, 2551–2555.
(10) Gur, I.; Fromer, N. A.; Geier, M. L.; Alivisatos, A. P. *Science* **2005**, *310*, 462–465.
(11) Johnston, K. W.; Pattantyus-Abraham, A. G.; Clifford, J. P.; Myrskog, S. H.; MacNeil, D. D.; Levina, L.; Sargent, E. H. *Appl. Phys. Lett.* **2008**, *92*, 151115.
(12) Redinger, D.; Molesa, S.; Shong, Y.; Farschi, R.; Subramanian, V. *IEEE Trans. Electron Devices* **2004**, *51*, 1978–1983.
(13) Peng, H. L.; Xie, C.; Schoen, D. T.; McIlwrath, K.; Zhang, X. F.; Cui, Y. *Nano Lett.* **2007**, *7*, 3734–3738.
(14) Peng, H.; Schoen, D. T.; Meister, S.; Zhang, X. F.; Cui, Y. *J. Am. Chem. Soc.* **2007**, *129*, 34–35.
(15) Xiao, J. P.; Xie, Y.; Xiong, Y. J.; Tang, R.; Qian, Y. T. *J. Mater. Chem.* **2001**, *11*, 1417–1420.
(16) Pan, D. C.; An, L. J.; Sun, Z. M.; Hou, W.; Yang, Y.; Yang, Z. Z.; Lu, Y. F. *J. Am. Chem. Soc.* **2008**, *130*, 5620–5621.
(17) Xiao, J. P.; Xie, Y.; Tang, R.; Qian, Y. T. *J. Solid State Chem.* **2001**, *161*, 179–183.
(18) Castro, S. L.; Bailey, S. G.; Raffaelle, R. P.; Banger, K. K.; Hepp, A. F. *J. Phys. Chem. B* **2004**, *108*, 12429–12435.
(19) Nairn, J. J.; Shapiro, P. J.; Twamley, B.; Pounds, T.; vonWandruszka, R.; Fletcher, T. R.; Williams, M.; Wang, C.; Norton, M. G. *Nano Lett.* **2006**, *6*, 1218–1223.

10.1021/ja809901u CCC: $40.75

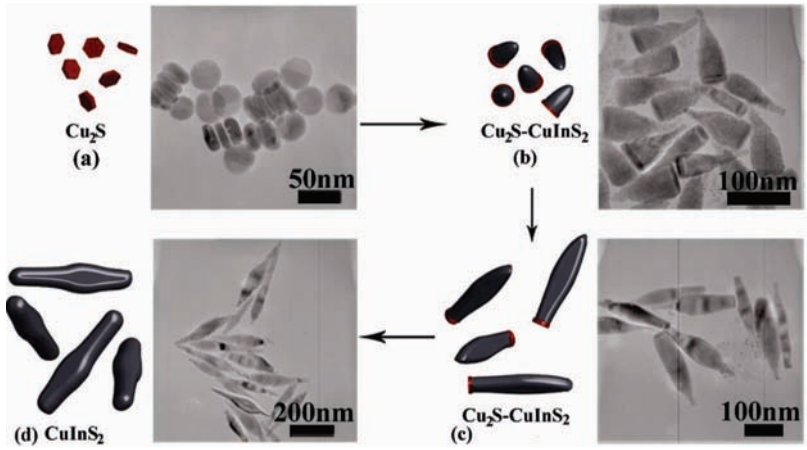

Figure 1. Schematic of the proposed growth mechanism with corresponding TEM images: (a) formation of Cu_2S nanodisks at the earliest times, (b) epitaxial growth of CISu on Cu_2S nanodisks leads to biphasic NRs, (c) continued growth of CISu occurs simultaneously with conversion of Cu_2S into CISu, (d) solely monophasic CISu present upon completion.

roquesite phase (JCPDS no. 85-1575), though Lu[16] has shown that a new wurtzite phase of CISu is accessible in their hot-injection synthesis method. The wurtzite phase allows flexibility of stoichiometry, due to the copper and indium sharing a lattice site. This is beneficial for device fabrication because it provides the ability to tune the Fermi energy over a wide range. A recent solvothermal synthetic procedure developed by Hyeon[20] and Tang[21] utilized metal oleate complexes in oleylamine and dodecanethiol to produce heterostructured nanocrystals. This method is attractive due to simplicity, low cost of precursors, and scalability of the synthesis; however, nanocrystals thus made were identified as $Cu_2S-In_2S_3$ heterostructures without CISu. Herein, we report that CISu nanocrystals can be synthesized under conditions similar to those of Hyeon[20] and Tang.[21] We discovered that the growth process starts with nucleation of Cu_2S nanodisks, followed by epitaxial overgrowth of CISu NRs onto only one side of the Cu_2S nanodisks, resulting in biphasic $Cu_2S-CISu$ heterostructured NRs. We also tracked the phase transformation of biphasic $Cu_2S-CISu$ heterostructured NRs into monophasic CISu over the synthesis time. We studied this complex phase behavior using a variety of characterization techniques including selected area electron diffraction (SAED), transmission electron microscopy (TEM), X-ray diffraction (XRD), UV−vis spectroscopy, and energy-dispersive X-ray spectroscopy (EDS).

Results and Discussion

Proposed Nanocrystal Growth Pathway. We studied the evolution of nanocrystal shape and composition during the reaction of copper oleate, indium oleate, dodecanethiol, and oleylamine, at 260 °C, by taking aliquots over the course of the reaction. Figure 1 shows a schematic representation summarizing growth steps along with corresponding TEM micrographs. Nanocrystals are proposed to first nucleate as Cu_2S nanodisks (diameters of 22 ± 5 nm and thicknesses of 9 ± 2 nm) (Figure 1a), followed by anisotropic overgrowth of wurtzite $CuInS_2$ onto only one side of the Cu_2S nanodisks. This forms biphasic $Cu_2S-CuInS_2$ heterostructured NRs (Figure 1b). As growth continues, the Cu_2S segment is chemically transformed into wurtzite $CuInS_2$, with an intermediate state seen in Figure 1c. At times after 20 min, the final monophasic $CuInS_2$ NRs are formed (Figure 1d). The NRs are tapered in shape, and the maximum diameter is found to be constant throughout the growth. The maximum diameter is found at the interface between the Cu_2S and CISu phases in the biphasic NRs and at the least tapered region in the monophasic NRs. All following analyses were performed on an aliquot taken at 5 min and the final product, which were chosen as representative samples of biphasic and monophasic nanoparticles, respectively.

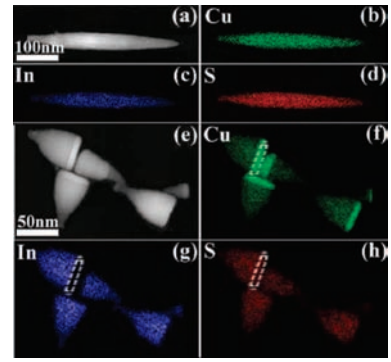

Figure 2. Electron images of (a) monophasic CISu and (e) biphasic $CISu-Cu_2S$ nanoparticles. EDS mapping of (b−d) monophasic CISu and (f−h) biphasic $CISu-Cu_2S$. A cap of a representative biphasic nanoparticle is highlighted with a white box for clarity. The intensity gradient in all biphasic nanoparticles is due to a corresponding thickness gradient of the cone-shaped bodies.

Elemental Mapping. EDS was performed with a JEOL 2100-F, in STEM (scanning transmission electron microscopy) mode, to determine the local composition of both the monophasic and biphasic nanocrystals. EDS mapping in Figure 2a−d shows that the monophasic CISu NRs grown for 20 min are elementally homogeneous along the whole NR within instrumental resolution. Parts e−h of Figure 2 are EDS mapping data of $Cu_2S-CuInS_2$ biphasic NRs grown for 5 min. Figure 2f shows that Cu is present throughout the NRs, but is in much higher concentrations in the caps of the NRs. However, the In signal in Figure 2g is located solely in the main body of the NRs, not at the cap, while the S signal is constant throughout the whole NR (Figure 2h). Large-area EDS on an FEI CM20 gives the Cu:In:S ratio in the monophasic CISu NRs as 23:27:50, which is close to the 1:1:2 ratio of CISu. The elemental ratio in the

(20) Choi, S. H.; Kim, E. G.; Hyeon, T. *J. Am. Chem. Soc.* **2006**, *128*, 2520–2521.
(21) Han, W.; Yi, L.; Zhao, N.; Tang, A.; Gao, M.; Tang, Z. *J. Am. Chem. Soc.* **2008**, *130*, 13152–13161.

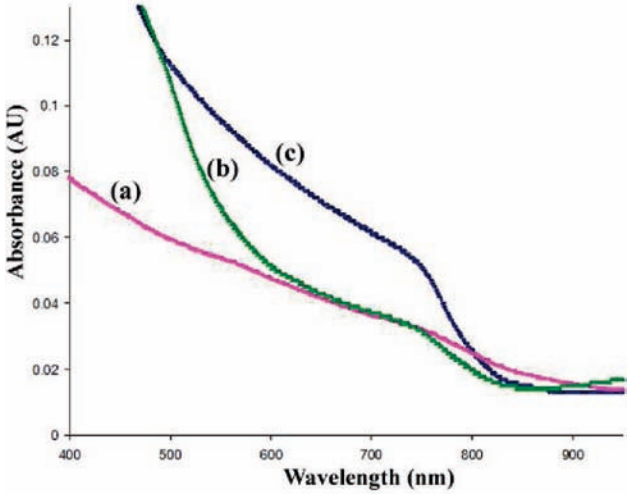

Figure 3. UV−vis spectra of (a) Cu_2S with a small CISu body, (b) CISu with a small Cu_2S cap, and (c) pure CISu nanoparticles in dilute toluene dispersions. Bulk band gap energies are 1.38 eV for Cu_2S and 1.5 eV for CISu.

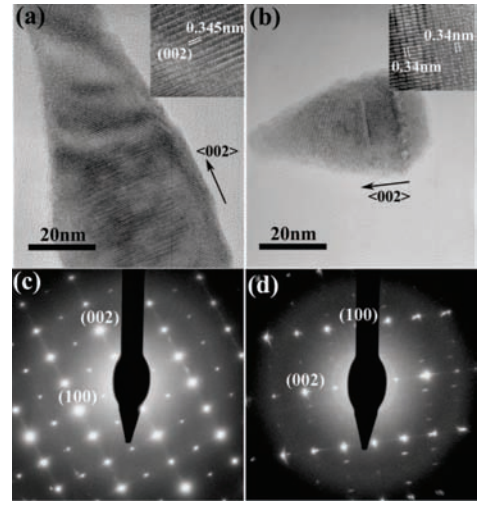

Figure 4. HRTEM images of (a) monophasic CISu and (b) Cu_2S−CISu nanoparticles with a phase boundary in the inset of (b). SAED of (c) monophasic CISu and (d) Cu_2S−CISu nanoparticles.

whole biphasic Cu_2S−CISu NPs is typically Cu-rich and In-poor by an amount corresponding to the cap volume, with a usual Cu:In:S ratio between 32:18:50 and 42:12:46. Elemental ratios of Cu:S in isolated copper sulfide nanodisks were found to be approximately 64:36, indicating that Cu_2S is present instead of CuS. It can be inferred from EDS mapping results that the chemical transformation involves the anisotropic interdiffusion of Cu and In between the Cu_2S and CISu phases, coupled with In absorption from solution and diffusion through the NR.

UV−Vis Spectroscopy. Spectroscopy was used to track the progression of Cu_2S−CISu NR growth via the optical band gap. We note that the nanocrystal size is much larger than the Bohr radius of these materials so that quantum confinement is not considered.[22] Figure 3a, the spectrum of a sample taken from a reaction at the first sign of color change, shows particles having a band gap of ∼1.38 eV (∼900 nm) (Figure S1a, Supporting Information), consistent with the band gap of Cu_2S in the chalcocite phases.[23] The spectrum of an aliquot at an intermediate stage of the reaction, in Figure 3b, shows the emergence of a shoulder at ∼1.63 eV (∼760 nm) (Figure S1b), indicating CISu nanocrystal formation. This shoulder is possibly from defect-based absorption,[18] and vacancies likely form during the low-temperature conversion process. Here, the shoulder is used as an indication of the progress of the growth of CISu and the biphasic to monophasic transition. The final product's spectrum in Figure 3c gives the band gap of CISu as ∼1.5 eV (∼830 nm) (Figure S1c). The stronger shoulder suggests the completion of the conversion to monophasic CISu nanoparticles.

High-Resolution Transmission Electron Microscopy (HRTEM) of Single Nanoparticles. HRTEM and SAED on monophasic CISu (Figure 4a,c) and biphasic Cu_2S−CISu (Figure 4b,d) nanocrystals give crystallographic information about the growth direction and relative orientation of the two phases. HRTEM and SAED of monophasic NRs are consistent with hexagonal wurtzite CISu with the NR long axis along the ⟨001⟩ direction. The SAED patterns of the biphasic nanoparticles in Figure 4d can be indexed as a hexagonal chalcocite Cu_2S phase (JCPDS no. 26-1116) and a hexagonal CISu phase. HRTEM shows the epitaxial interface between Cu_2S and CISu. Both Cu_2S and CISu have the same ⟨001⟩ crystallographic direction pointing along the long axis of the NRs. We note that there are only 4% and 1.5% differences in the *c* and *a* lattice parameters, respectively, between Cu_2S and CISu, so the epitaxial interface is expected. In a fashion similar to that of other ternary chalcogenide nanostructures,[14] both monophasic and biphasic nanoparticles show evidence of 2- or 4-fold superlattice formation in the ⟨100⟩ direction, as seen in Figure 4c,d. Superlattice formation can be indicative of extensive defect formation in ternary chalcogenides.[13,24] Defect formation would allow anisotropic vacancy-based diffusion,[25] which can contribute to the generation of one-dimensional structures, along with parallel mechanisms such as differential surfactant absorption between crystal faces, as seen in CdSe nanocrystal growth.[26]

X-Ray Diffraction. Our TEM and SAED analysis is supported by XRD in Figure 5a, which also shows that the CISu NRs can be indexed as the wurtzite phase. Figure 5b shows a simulated powder diffraction pattern generated from the proposed CISu structure of Lu,[16] which agrees in intensity and position with the experimental pattern. While a combination of the tetragonal In_2S_3 and hexagonal Cu_2S reference patterns in Figure 5c,d can approximate some of the peaks, the match is weak and has several extraneous reflections.

Epitaxial Growth and Phase Conversion. The most interesting elements of our growth process are the nucleation of Cu_2S nanodisks, epitaxial overgrowth of CISu, and phase conversion of Cu_2S into CISu so that biphasic Cu_2S−CISu NRs can turn into monophasic CISu NRs. There are several interesting points about the conversion mechanism. First, CISu and Cu_2S both have a hexagonal structure and share nearly identical packing of the S sublattices. Parts a and b of Figure 6 show the crystal

(22) Czekelius, C.; Hilgendorff, M.; Spanhel, L.; Bedja, I.; Lerch, M.; Müller, G.; Bloeck, U.; Su, D.-S.; Giersig, M. *Adv. Mater.* **1999**, *11*, 643–646.
(23) Kuzuya, T.; Itoh, K.; Ichidate, M.; Wakamatsu, T.; Fukunaka, Y.; Sumiyama, K. *Electrochim. Acta* **2007**, *53*, 213–217.
(24) Tham, A.-T.; Su, D. S.; Neumann, W.; Schubert-Bischoff, P.; Beilharz, C.; Benz, K. W. *Cryst. Res. Technol.* **2001**, *36*, 303–308.
(25) Konstantin, G.; Leonid, C.; Vera, L.; David, C.; Vladimir, D.; Vitaliy, K.; Roald, M.; Elena, S.; Valentina, U. *J. Appl. Phys.* **1997**, *82*, 4282–4285.
(26) Manna, L.; Wang, L. W.; Cingolani, R.; Alivisatos, A. P. *J. Phys. Chem. B* **2005**, *109*, 6183–6192.

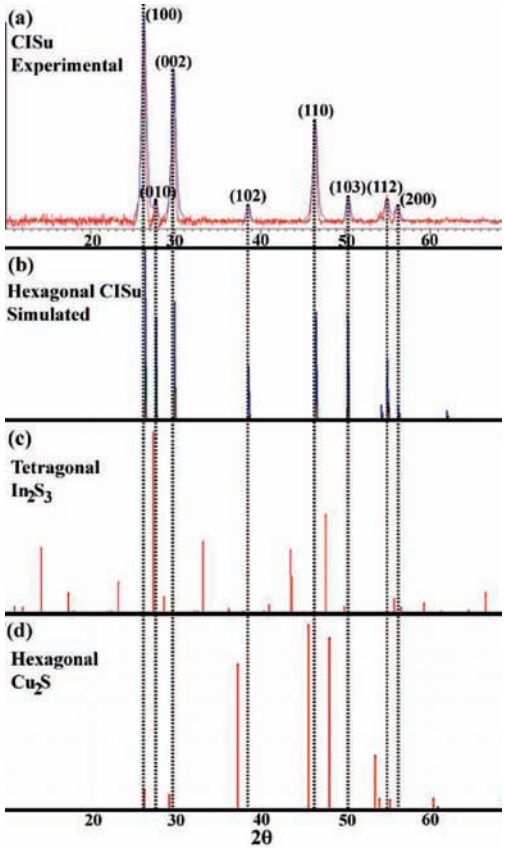

Figure 5. (a) Experimental XRD pattern of CISu nanoparticles. (b) Simulated powder diffraction of proposed hexagonal CISu structure. Reference patterns of (c) tetragonal In_2S_3 and (d) hexagonal Cu_2S. Guidelines overlaid to demonstrate matching of (a) with (b) and mismatching of (a) with (c) and (d).

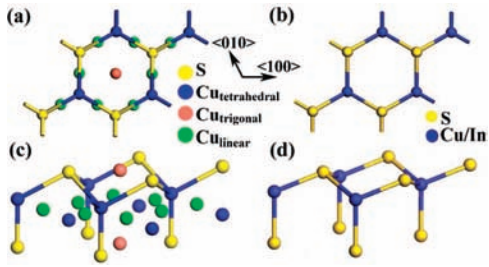

Figure 6. Crystal structure of (a) hexagonal chalcocite Cu_2S and (b) hexagonal CISu with a zone axis of ⟨001⟩. Crystal structure of (c) hexagonal chalcocite Cu_2S and (d) hexagonal CISu viewed from another angle.

structures of Cu_2S and CISu, respectively, projected along the ⟨001⟩ direction. Parts c and d of Figure 6 show the crystal structure from an isometric point of view roughly along the ⟨110⟩ direction for Cu_2S and CISu. For Cu_2S, the Cu(I) ions are color-coded to indicate different S coordinations: tetrahedral (blue), trigonal (red), and linear (green). Second, at the growth temperature of 250 °C, the chalcocite Cu_2S phase is in the superionic conducting state.[27] Cu(I) ions are randomly distributed in the interstitial sites formed by the S sublattice. Cu(I) ions have very high mobility, as if they are in a fluidic state, which speeds up exchange with In(III) ions and chemical transformation. Third, the conversion from Cu_2S to CISu requires little lattice distortion and thus can be done with a low-

(27) Wakamura, K.; Tsubota, I. *Solid State Ionics* **2000**, *130*, 305–312.

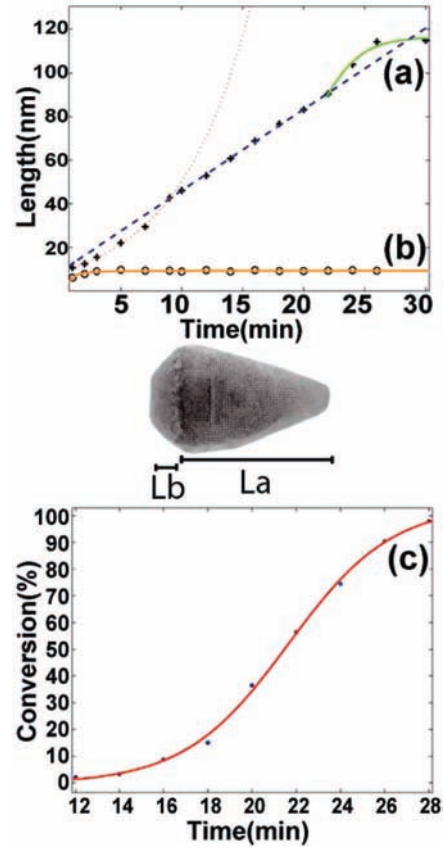

Figure 7. Time traces of (a) CISu length L_a (nm), (b) Cu_2S thickness L_b (nm), and (c) conversion progress (monophasic nanoparticles/total nanoparticles, %). Fittings are (a) exponential, linear, and logistic, (b) a power law, and (c) sigmoidal ($\ln(100 - \text{conversion}/\%) = kt^n$ with $n = 4$).

energy barrier. As visualized in Figure 6, the S sublattices do not need to move while half of the Cu(I) ions (trigonally and linearly bonded Cu(I) ions) are required to move out of the Cu_2S phase.[28] Half of the remaining Cu(I) ions (tetrahedrally bonded) are replaced by In(III) ions. Finally, both Cu(I) and In(III) ions randomly distribute among tetrahedral sites, resulting in the CISu phase.

Growth Mechanism. Understanding the growth mechanism can allow precise control over the size and shape of resultant nanoparticles. This reaction can be modeled as three separate steps: the nucleation of Cu_2S nanodisks, the growth of the CISu phase on only one side of the Cu_2S nanodisks through absorption of reactants, and the conversion from biphasic to monophasic nanocrystals by interdiffusion of Cu and In between the CISu and Cu_2S phases. The progressions of growth in the CISu NR length and Cu_2S nanodisk thickness and phase transformation with respect to time are shown in Figure 7. The seemingly linear increase in the CISu NR length, seen in the blue curve of Figure 7a, can be described as diffusive growth in one dimension with a constant concentration of precursors.[29] However, the detailed time trace also shows a slight exponential at times between 0 and 9 min (red curve of Figure 7a), caused by the limiting step of forming Cu_2S seeds at early times. The depletion of Cu and In reactants also causes the length to reach a saturation limit at later times between 22 and 30 min (green curve of Figure 7a). This shape is commonly seen for fast nucleation steps followed

(28) Buerger, M. J.; Wuensch, B. J. *Science* **1963**, *141*, 276–277.
(29) Peng, Z. A.; Peng, X. *J. Am. Chem. Soc.* **2002**, *124*, 3343–3353.

by diffusive growth,[30] but the middle linear growth stage is prolonged due to the high stability of the metal oleate precursors. Their stability at high temperatures leads to a low and constant concentration of active metal species in solution, which in turn leads to a constant rate of NR elongation as seen in the middle linear region of Figure 7a.

The disappearance of the Cu_2S phase also occurs at later times and is modeled here as a solid-state phase change. Progress is tracked, in Figure 7c, as the fraction of the number of monophasic to total nanocrystals versus the same reaction time as in Figure 7a,b. This transformation occurs concurrently with the saturation of CISu growth at around 20 min, likely due to a reduction in the concentration of copper oleate in solution. The only source of Cu at subsequent times is the Cu_2S phase, though it does not seem that Cu is gradually leeched, but is instead suddenly removed. The surprising abruptness of this transition is reflected in the constant Cu_2S nanodisk thickness prior to transformation, as seen in Figure 7b, which coincided with the absence of partially transformed Cu_2S nanodisks. We think that the abruptness of the transition is due to the thinness (9 nm) of the Cu_2S phase and the high Cu ion mobility in the superionic state. The curve in Figure 7c can then be fit well to the Avrami−Erofe'ev growth model,[31,32] which simulates a solid−solid seed-based phase transformation with an estimated order of ~4 by least-squares fitting. This indicates that the transition is likely three-dimensional despite the linearity of the NRs and involves a high rate of nucleus generation at the CISu−Cu_2S interface, which would corroborate the sudden disappearance of the Cu_2S phase.

The original causes of one-dimensional growth are likely the inhibition of radial diffusion by the surfactant oleylamine and enhancement of growth rates at the high-energy (001) faces of wurtzite chalcogenides.[33] The fact that CISu only nucleates onto one side of the Cu_2S nanodisks suggests that the (001) face terminated with S anions has a binding affinity different from that of the face terminated with Cu and In cations. In this study, it is not yet determined which face favors the CISu overgrowth. Our observation of preferential growth of one side of a nanocrystal has previously been seen in the case of wurtzite CdSe NRs,[29,34] which showed preferential growth on the cationic (001) face, leading to a "tadpole" shape. Our system's novel combination of stable precursors, well-separated nucleation and growth steps, and asymmetric crystal structure provides an easily analyzed and controlled growth of one-dimensional CISu nanoparticles.

Conclusions

We have synthesized a range of Cu−In−S structures, with fine control over both phase and size, by a low-temperature solution-phase synthesis. We found that the growth process starts with Cu_2S nanodisks followed by epitaxial overgrowth of $CuInS_2$ on only one side of the nanodisks, resulting in biphasic Cu_2S−$CuInS_2$ heterostructures consisting of hexagonal chalcocite Cu_2S and wurtzite $CuInS_2$. We showed that the biphasic NRs can be easily converted to monophasic NRs at temperatures above 250 °C due to their similar crystal structures and fast diffusion of Cu(I) ions in the superionic state. These compositional, structural, and mechanistic findings provide valuable insight into the controlled solution growth of ternary chalcogenide nanoparticles and will aid in the development of solar cells using ternary I−III−VI_2 semiconductors.

Experimental Section

All chemicals were used as purchased from Sigma-Aldrich, and rigorous air exclusion techniques were employed by means of a Schlenk line with argon gas.

Preparation of Oleate Precursors. Indium and copper oleates were synthesized by the ion exchange of 20 mmol of sodium oleate with 10 mmol of copper chloride or 30 mmol of sodium oleate and 10 mmol of indium chloride in 35 mL of hexane, 15 mL of water, and 20 mL of ethanol. The reaction mixture was heated at 60 °C and stirred vigorously for 4 h, followed by repeated cleanings with water and evaporation of residual hexane.

Synthesis of Cu−In−S Nanoparticles. In a typical synthesis, 0.16 mmol of copper oleate and 0.2 mmol of indium oleate were mixed with 5 mL of dodecanethiol and 5 mL of oleylamine in a three-neck flask, and the solution was vacuumed at room temperature for 20 min and at 100 °C for 20 min. The reaction mixture was then put under an argon atmosphere and heated to a temperature between 215 and 300 °C for 20 min; cooling to room temperature was allowed to occur gradually under an argon atmosphere. Biphasic nanoparticles were obtained at temperatures below 250 °C or at early times (<5 min) at higher temperatures. The product was dispersed into ethanol and centrifuged four times to wash out unreacted precursors and contaminants. The nanoparticles were then dispersed in toluene, where they remained suspended for several days, and were easily redispersed by sonication. Small amounts of bulk Cu_2S were found to be present in samples with excesses of copper oleate, but they could be filtered out with PTFE filters with 450 nm pores.

Transmission Electron Microscopy. TEM was primarily performed on an FEI CM20 at the Stanford Nanocharacterization Laboratory (SNL) at Stanford University. Additional imaging and elemental mapping by EDS were performed on a JEOL 2100-F at the Molecular Foundry's Imaging Facility at Lawrence Berkeley National Laboratory. TEM samples were prepared by drop-casting dispersion onto nickel grids, followed by repeated washings in acetone, methanol, and ethanol.

X-Ray Diffraction. XRD was performed at the SNL on a PANalytical X'Pert with Cu Kα radiation at 45 kV and 40 mA, and crystal modeling and XRD simulation were done with Materials Studio at the SNL. XRD samples were drop-cast out of toluene, and all films showed no changes due to oxidation over several weeks in the atmosphere.

UV−vis Spectroscopy. UV−vis spectra were collected on a Shimadzu UV-1700. The band gap determination methodology can be found in the Supporting Information. Samples were diluted into toluene, and spectra were taken in a two-beam transmission mode with pure toluene as the reference.

Acknowledgment. Y.C. acknowledges support from the U.S. Department of Energy under Award Number DE-FG36-08GO18005 and from the Stanford Global Climate and Energy Project. S.T.C. acknowledges support from a National Science Foundation Graduate Fellowship. The work is also supported by the User Program in Molecular Foundry, Lawrence Berkeley National Laboratory, under Contract No. DE-AC02-05CH11231.

Supporting Information Available: Fitting of UV/vis spectra and XRD pattern of Cu_2S−CISu biphasic nanoparticles. This material is available free of charge via the Internet at http://pubs.acs.org.

JA809901U

(30) Robb, D. T.; Privman, V. *Langmuir* **2008**, *24*, 26–35.
(31) Francis, R. J.; O'Brien, S.; Fogg, A. M.; Halasyamani, P. S.; O'Hare, D.; Loiseau, T.; Ferey, G. *J. Am. Chem. Soc.* **1999**, *121*, 1002–1015.
(32) Avrami, M. *J. Chem. Phys.* **1939**, *7*, 1103–1112.
(33) Zhao, L.; Lu, T.; Yosef, M.; Steinhart, M.; Zacharias, M.; Gosele, U.; Schlecht, S. *Chem. Mater.* **2006**, *18*, 6094–6096.
(34) Manna, L.; Scher, E. C.; Alivisatos, A. P. *J. Am. Chem. Soc.* **2000**, *122*, 12700–12706.